*Chapter-3*

# NUCLEUS-ACOUSTIC WAVE DYNAMICS IN GYROGRAVITATING ELECTROSPHERICALLY CONFINED DEGENERATE QUANTUM PLASMAS

***Abstract:*** *A theoretic model is presented to investigate the excitation and propagation dynamics of the nucleus-acoustic waves in a gyrogravitating electrostatically confined degenerate quantum plasma system*[†]*. We consider a three-component spherically symmetric degenerate quantum plasma system, comprising of non-degenerate heavy nuclear species, light nuclear species, and degenerate electronic species. It is under the conjoint influence of the Bohm potential, Coriolis rotation, viscoelasticity, electrostatic confinement pressure, self-gravity, and so on. A standard normal spherical mode analysis yields a generalized linear dispersion relation (septic in degree). The dispersion coefficients have plasma multiparametric influences in an atypical fashion. We numerically illustrate and interpret various stabilizing and destabilizing factors extensively relevant in compact astro-environs.*

## 3.1 INTRODUCTION

The area of quantum plasmas is one of the most rapidly growing research fields owing to its large-scale potential applications [1-4]. While traditional classical plasmas revolve around regions of low density and high temperature, quantum plasmas are characterized by high particle density ($\sim 10^{29} - 10^{36}$ $m^{-3}$) and low temperature ($T \sim T_F$) [1, 2, 4]. Widespread occurrence of such plasma is found in white dwarfs, brown dwarfs, neutron stars, and so on [4, 5]. Under extreme conditions of temperature and density, these qualify as degenerate quantum plasma systems. The degeneracy of these systems stem primarily from the combined action of the Pauli exclusion principle and the Heisenberg uncertainty principle [6-8]. According to Pauli exclusion principle, no two fermions can have all four set of quantum numbers identical. The fermionic particles are highly uncertain in their momenta as a result of their locations in highly confined phase space. As a result, when the electrons are subjected to extreme pressure of the highly dense

[†]Dasgupta, S. and Karmakar, P. K. Propagatory dynamics of nucleus-acoustic waves in gyrogravitating degenerate quantum plasmas electrostatically confined in curved geometry. *Scientific Reports*, 11:19126, 2021.

quantum plasma systems, they exert a very high counter quantum pressure known as the electron degeneracy pressure [9, 10].

It is a well-known fact that white dwarfs are supported against gravity by the electron degeneracy pressure. Several studies have been conducted that highlight the fact that white dwarfs are composed of degenerate electronic species, weakly coupled light nuclear species (mostly hydrogen (H) and helium (He)), and strongly coupled heavy nuclear species (mostly carbon (C) and oxygen (O)) [11-13]. Electrons are relativistically degenerate within the inner core and non-relativistically degenerate in the outer mantle [1, 2]. Presence of particles of different masses has interactions among them, leading to excitation of different kinds of waves and instabilities. Nucleus-acoustic waves are the propagatory longitudinal oscillations that arise as a result of the interplay between the elasticity contributed conjointly by the degenerate electronic species and light nuclear species, and inertial force provided by the heavy nuclear species [1]. The elasticity contributed by the electronic species is found to be significantly higher than the light nuclear species [1]. As such, nucleus-acoustic waves get excited essentially due to the elasticity of the lighter electronic species and inertia of the heavier nuclear species [1]. In other words, such modes are the rhythmic outcomes of any perturbation in the inertial nuclear fluid existing in a stable hydrostatic equilibrium with the non-inertial degenerate lighter ones acting as restoring agents in the composite plasma system. There exist a good number of investigations dealing with the nucleus-acoustic waves and non-linear structures associated with them [14-23]. However, very few studies have been dedicated to explore the linear dynamics of the nucleus-acoustic waves in the presence of realistic key parameters actually found in naturalistically occurring degenerate quantum plasma systems. In this context, one could not ignore the role of the quantum-mechanical diffraction effects (Bohm potential), gyration effects (Coriolis), non-thermal (electrostatic) confinements, etc.

In the present study, we consider a three-component spherically symmetric degenerate quantum plasma system to investigate the linear excitation of the nucleus-acoustic waves. The consideration of spherical geometry can be justified on the grounds that most of the astrophysical bounded structures, like white dwarfs, brown dwarfs, etc. are spherical in shape. The considered system comprises of the degenerate electronic species, weakly coupled light-nuclear species, and strongly-coupled heavy nuclear species. Real astronomic evidences are present that highlight the actual composition of

white dwarfs to be similar to the considered composition. It evolves under the conjoint influence of the electrostatic confinement pressure [24], Bohm potential, Coriolis rotational force [25-26], viscoelasticity [28-29], self-gravity [27-29], and so on. Out of all the considered parameters, it is the electrostatic confinement pressure, scaling quadratically with number density, which has been considered in similar circumstances for the first time. It is assumed that in white dwarfs, the light and heavy nuclear species are confined in the system by means of their auto-generated electric fields [24]. As such, these mean electric fields contribute appreciably to the total pressure of the system [24]. Thus, the inclusion of the electrostatic confinement pressure becomes of utmost importance in the considered model set up. A significant fraction of white dwarfs have been observationally reported to show rotation [25, 26]. It is noteworthy herein that the angular momentum of the white dwarfs have primordial origin [25-27]. The effects considered in the current study have been found to significantly influence the white dwarf characteristics [30-34]. The practical realization of such a correlated physical plasma system could be achieved in the interiors of white dwarf stars, particularly the CO white dwarfs, having the asymptotic mass scaling in the range $0.25M_{\odot} < M < 8M_{\odot}$; where, $M_{\odot} = 1.98 \times 10^{30}$ kg is the mass of the Sun [35]. The simultaneous realistic effects considered here are mainly applicable to rapidly rotating collapsing white dwarfs [33]. It also finds applicability in the viscous evolution of remnants of white dwarf mergers, leading to detonation of their He envelope [34]. Thus, the considered model has widespread applicability to analyze the wave excitation dynamics in dwarf stars, like the white dwarfs, brown dwarfs, and their associated environments.

### 3.2 PHYSICAL MODEL AND FORMALISM

We consider a gyrogravitating degenerate electrostatically confined quantum plasma system, consisting of strongly coupled heavy nuclear species, weakly coupled light nuclear species, and non-relativistic and ultra-relativistic degenerate electronic species. The electronic species is treated quantum-mechanically, whereas, the light and heavy nuclear species are given classical treatment. We use a generalized hydrodynamic formalism to model the dynamics of the system. The considered model set up evolves under the simultaneous influence of the Bohm potential, Coriolis rotation, electrostatic

confinement pressure, viscoelasticity, and self-gravity. The basic equations governing the model are the flux conservation continuity equation, force-balancing momentum equation, and appropriate equations of state for each of the three constitutive species [1, 2, 7, 24]. The model is systematically closed with the help of the electrostatic and gravitational Poisson equations. The equations governing the electronic dynamics, in their customary notations [1, 7], are respectively cast as

$$\partial_t n_e + r^{-2}\partial_r\left(r^2 n_e u_e\right) = 0\,, \tag{3.1}$$

$$e\partial_r \Phi - n_e^{-1}\partial_r P_e - \hbar^2\left(2m_e\right)^{-1}\partial_r\left(n_e^{-\frac{1}{2}}\right)\left[r^{-2}\partial_r\left\{r^2\partial_r\left(n_e^{-\frac{1}{2}}\right)\right\}\right] = 0\,, \tag{3.2}$$

$$P_e = K_e\, n_e^{\gamma_e}\,. \tag{3.3}$$

Likewise, the equations governing the dynamics of the light nuclear species [1, 2, 7, 24] are cast as

$$\partial_t n_l + r^{-2}\partial_r\left(r^2 n_l u_l\right) = 0\,, \tag{3.4}$$

$$\left(\partial_t + u_l\,\partial_r\right)u_l + \left(eZ_l m_l^{-1}\right)\partial_r\Phi + \partial_r\psi + \left(m_l n_l\right)^{-1}\partial_r P_l = 0\,, \tag{3.5}$$

$$P_l = n_l k_B T + B_l\, n_l^2\,. \tag{3.6}$$

The heavy nuclear species dynamics [1, 2, 7, 24, 36, 37] can analogously be cast as

$$\partial_t n_h + r^{-2}\partial_r\left(r^2 n_h u_h\right) = 0\,, \tag{3.7}$$

$$\begin{aligned}&\left[1+\tau_m\left(\partial_t + u_h\partial_r\right)\right]\left[\left(\partial_t + u_h\partial_r\right)u_h + \left(eZ_h m_h^{-1}\right)\partial_r\Phi + \partial_r\psi + 2\Omega_\phi v_\theta + \left(m_h n_h\right)^{-1}\partial_r P_h\right]\\ &= \left(m_h n_h\right)^{-1}\left(\zeta + 4(3)^{-1}\eta\right)r^{-2}\partial_r\left(r^2\partial_r u_h\right)\,,\end{aligned} \tag{3.8}$$

$$P_h = n_h k_B T + B_h\, n_h^2\,. \tag{3.9}$$

The system closing electrostatic and gravitational Poisson equations, in their generic notations [1, 2, 7] are respectively given as

$$r^{-2}\partial_r\left(r^2\partial_r\Phi\right)=\left(e/\varepsilon_0\right)\left(n_e-Z_l n_l-Z_h n_h\right), \tag{3.10}$$

$$r^{-2}\partial_r\left(r^2\partial_r\psi\right)=\left(4\pi G\right)\left(\Delta\rho_l+\Delta\rho_h\right). \tag{3.11}$$

The notation $n_s$ stands for the population density associated with the *s*th species; *s* being *e* for the electrons, *l* for light nuclear species, and *h* for heavy nuclear species. $Z_s$, $m_s$, $P_s$, $u_s$ signify the charge state, mass, pressure and flow speed of the *s*th species (*s* = *e*, *l*, *h*). *T* signifies the temperature of the system (in K). $B_l$ and $B_h$ are the electrostatic confinement constants associated with the light and heavy nuclear species, respectively. The azimuthal component of the angular velocity and polar component of the rotational velocity are respectively denoted as $\Omega_\phi$ and $v_\theta$. $\Phi$ represents the electrostatic potential. $\psi$ is the gravitational potential. $k_B = 1.38\times10^{-23}$ J K$^{-1}$ is the Boltzmann constant signifying the energy-temperature coupling. $G = 6.67\times10^{-11}$ N m$^2$ kg$^{-2}$ is the universal gravitational constant through which gravitating matter interacts. $\zeta$ and $\eta$ are the bulk viscosity (resistance to transverse flow) and shear viscosity (resistance to longitudinal flow) coefficients, respectively. $\tau_m$ is the viscoelastic relaxation time of the strongly coupled heavy nuclear fluid. $\Delta\rho_l = \rho_l - \rho_{l0} = m_l\left(n_l - n_{l0}\right)$ and $\Delta\rho_h = \rho_h - \rho_{h0} = m_h\left(n_h - n_{h0}\right)$ have been used to model the Jeans swindle.

A number of points regarding the above equations are noteworthy. Equation (3.1) denotes the equation of continuity for the degenerate electronic species. Equation (3.2) signifies the force-balancing momentum equation, wherein the forces by virtue of the electrostatic potential, degenerate pressure, and Bohm potential exactly balance each other. It should be noted that the Bohm potential term only appears in the momentum equation for the electronic species because in the current model set up, only the electronic species is treated quantum-mechanically. The physical reason behind this can be ascribed to the fact that the quantum behaviour becomes significant when the

interparticle distance becomes of the order of the de-Broglie wavelength ($\hbar/mv$). As such, the quantum behaviour is reached much easily for the electrons as compared to the light and heavy nuclear species, owing to the extremely small mass of the electronic species. The Bohm potential term accounts for the quantum-like behaviour, like tunneling, wave-packet spreading, and so on. Equation (3.3) is the equation of state for the electronic species, accounting for their degeneracy pressure. The polytropic pressure law given as: $P_e = K_e\, n_e^{\gamma_e}$ ; where, the polytropicity constant, $K_e = 3\lambda_C \hbar c/5$ (with $\lambda_C = \pi\hbar/m_e c$), and the polytropicity exponent, $\gamma_e = 5/3$, for the non-relativistic limit. This is in contrast with the ultra-relativistic limit with their corresponding counterparts, given as, $\gamma_e = 4/3$ and $K_e = 3\hbar c/4$ [9, 10]. Equation (3.4) gives the equation of continuity for the light nuclear species. Equation (3.5) gives the force-conservation momentum equation for the light nuclear species where the forces by virtue of their motion, electrostatic potential, gravitational potential, and pressure exactly balance each other. Equation (3.6) is the equation of state for the light nuclear species, taking into account the classical thermal pressure and the electrostatic confinement pressure, scaling quadratically with density. Equation (3.7) is the exact analog of equations (3.1) and (3.4). Equation (3.8) is the force-balancing momentum equation for the heavy nuclear species where the various forces exerted by virtue of their motion, electrostatic potential, gravitational potential, composite pressure, and Coriolis rotation are exactly balanced by the dissipative viscoelastic forces. Equation (3.9) is the analog of equation (3.6), but for the heavy nuclear species giving sum of the classical thermal pressure and the electrostatic confinement pressure. The model configuration is closed with the electrostatic and gravitational Poisson equations, given by equations (3.10) and (3.11).

The difference in forms of the equations of state of the electronic species (equation (3.3)) and light (equation (3.6)), and heavy nuclear species (equation (3.9)) can be physically ascribed to the fact that in dwarf plasmas, the degenerate pressure of the electrons far exceeds all other pressures acting on the species, such as the electron thermal pressure, electrostatic confinement pressure, etc. It hereby makes the degenerate electron pressure significantly prevail only on the quantum degenerate electronic species (equation (3.3)). Another important point that should be mentioned herein is that there is a significant difference in the mathematical forms of the force-balancing equations of the light nuclear species (equation (3.5)), and heavy nuclear species

(equation (3.8)), respectively. In order to explain the difference, it is noteworthy to mention the Coulomb coupling parameter. In simple terms, the Coulomb coupling parameter [38, 39], that is $\Gamma$, is defined as the ratio of the mean potential energy per particle to the mean kinetic energy per particle. For classical particles, $\Gamma = \left(Ze^2\right) / ak_B T$; where, $a \propto n^{-1/3}$ is the interparticle separation [7, 38]. It is evident that $\Gamma > 1$ for the heavy nuclear species due to their high charge and low temperature. Thus, the heavy nuclear species are strongly coupled. The fact that kinetic energy of the heavy nuclear species is comparatively low owing to their higher mass also adds to the reasons behind the heavy nuclear species for being strongly coupled. Similarly, $\Gamma < 1$ for the light nuclear species on account of their higher kinetic energy than the heavy species. In other words, the light nuclear species are weakly coupled. Viscoelastic behaviour is exhibited by only the strongly coupled fluid in the range $1 < \Gamma < \Gamma_c$ ($\Gamma_c$ is the critical limit beyond which the fluid crystallizes) [38]. Thus, the viscoelastic terms are included only in the momentum equation of the strongly coupled heavy nuclear species. Again, mathematically, the Coriolis rotational force is given as $F_C = 2m\left|\left(\vec{v} \times \vec{\omega}\right)\right|$. Clearly, the rotational part, $\left|\left(\vec{v} \times \vec{\omega}\right)\right|$, is constant for a uniformly rotating plasma system. Thus, the effect of the Coriolis rotation becomes extremely small for the tiny electrons with negligible mass. Due to similar reasons, the rotational term has been neglected in the momentum equation of the light nuclear species (equation (3.5)) as well.

In order for a scale-invariant analysis of the proposed model [1, 2, 7, 24], we apply a standard astronormalization scheme to obtain a dimensionless set of normalized governing equations cast as

$$\partial_\tau N_e + \xi^{-2} \partial_\xi \left(\xi^2 N_e M_e\right) = 0 , \tag{3.12}$$

$$N_e \partial_\xi \Phi_E - K_e' \gamma_e N_e^{\gamma_e - 1} \partial_\xi N_e - 2^{-1} H'^2 M_{Fe}^2 \left[2^{-1} \partial_\xi^3 N_e + \xi^{-1} \partial_\xi^2 N_e - \xi^{-2} \partial_\xi N_e\right] = 0, \tag{3.13}$$

$$\partial_\tau N_l + \xi^{-2} \partial_\xi \left(\xi^2 N_l M_l\right) = 0 , \tag{3.14}$$

$$\left(\partial_\tau + M_l\partial_\xi\right)M_l N_l + N_l\partial_\xi\Phi_E + N_l\partial_\xi\Psi + A_l'\partial_\xi\left[N_l T^* + B_l^* N_l^2\right] = 0, \tag{3.15}$$

$$\partial_\tau N_h + \xi^{-2}\partial_\xi\left(\xi^2 N_h M_h\right) = 0\,, \tag{3.16}$$

$$\left[1+\tau_m^*\partial_\tau\right]\left[\left(\partial_\tau + M_h\partial_\xi\right)M_h N_h + \beta N_h\partial_\xi\Phi_E + N_h\partial_\xi\Psi + 2N_h C_F^* + A_h'\partial_\xi\left(N_h T^* + B_h^* N_h^2\right)\right]$$
$$= \chi^*\xi^{-2}\partial_\xi\left(\xi^2\partial_\xi M_h\right), \tag{3.17}$$

$$\xi^{-2}\partial_\xi\left(\xi^2\partial_\xi\Phi_E\right) = (1+\mu)N_e - N_l - \mu N_h\,, \tag{3.18}$$

$$\xi^{-2}\partial_\xi\left(\xi^2\partial_\xi\Psi\right) = \sigma\left\{(N_l - 1) + \mu\beta^{-1}(N_h - 1)\right\}, \tag{3.19}$$

where, $\xi = r/\lambda_{Dl}$ is the normalized radial coordinate with the normalization parameter given as $\lambda_{Dl} = \left(m_e c^2/n_{l0}Z_l e^2\right)^{1/2}$. $\lambda_{Dl}$ is the light nuclear Debye length scale. $\tau = t/\omega_{pl}^{-1}$ is the normalized time coordinate. $\tau_m^* = \tau_m/\omega_{pl}^{-1}$ is the normalized viscoelastic relaxation time. The time normalization factor is the light nuclear plasma oscillation time scale given as: $t_{pl} = \omega_{pl}^{-1} = \left(m_l/n_{l0}Z_l^2 e^2\right)^{1/2}$. $Z' = Z_h/Z_l$ denotes the ratio of the heavy-to-light nuclear charge number. $\mu = Z' n_{h0}/n_{l0}$ stands for the ratio of the charge densities of the heavy-to-light nuclear species. The relative nuclear charge-to-mass coupling parameter is denoted by $\beta = Z' m_l/m_h$. The population densities of the constitutive particles have been normalized by their equilibrium number density as $N_s = n_s/n_{s0}$. The squared Fermi Mach number is given by $M_{Fe}^2 = v_{Fe}^4/C_l^2 c^2$. Likewise, the normalized form of the fluid flow velocity is given by $M_s = u_s/C_l$, where $C_l = \left(Z_l\, m_e c^2/m_l\right)^{1/2}$ gives the light nuclear transit speed. $H' = \hbar\omega_{pl}/m_e\, v_{Fe}^2$ denotes the quantum parameter signifying the ratio between the plasmon energy associated with the light nucleus and the Fermi energy associated with degenerate electrons. The ratio between the square of the Jeans frequency to that of the light nuclear plasma oscillation frequency is given as $\sigma = \omega_{Jl}^2/\omega_{pl}^2$, where $\omega_{Jl} = \sqrt{4\pi G n_{l0} m_l}$. $A_l' = m_e c^2/m_l\, C_l^2$ stands for the ratio of the

relativistic electronic energy to the light nuclear species energy. $A_h' = m_e c^2 / m_h C_l^2$ is the analog for the heavy nuclear species. The constants $B_l^*$ and $B_h^*$ have been normalized as $B_l^* = B_l n_{l0} / m_e c^2$ and $B_h^* = B_h n_{h0} / m_e c^2$, respectively. $T^* = k_B T / m_e c^2$ stands for the normalized isothermal nuclear plasma temperature of the bulk plasma fluid. The effective generalized viscosity given by $\chi = (\zeta + 4\eta/3)$ has been normalized as $\chi^* = \chi / m_h n_{h0} C_l \lambda_{Dl}$. The normalized polytropic constant for the electronic dynamics is given as $K_e' = K_e n_{e0}^{\gamma_e - 1} / m_e c^2$. The normalized Coriolis force is denoted as $C_F^* = \Omega_\phi^* M_{h\theta}$, where the azimuthal component of angular velocity and polar component of the rotational velocity are normalized as $\Omega_\phi^* = \Omega_\phi / \omega_{pl}$ and $M_{h\theta} = v_\theta / C_l$, respectively. $\Phi_E = e\Phi / m_e c^2$ is the normalized electrostatic potential arising due to local plasma polarization effects. The normalized gravitational potential is given as $\Psi = \psi / C_l^2$.

### 3.3 LINEAR STABILITY ANALYSIS

The relevant physical fluid parameters in equations (3.12)-(3.19) are linearly perturbed ($F_1$) about their homogeneous equilibrium values ($F_0$) using a standard normal spherical mode analysis in an autonormalized Fourier form as

$$F(\xi, \tau) = F_0 + F_1 = F_0 + F_{10}(\xi^{-1}) \exp\left[-i(\Omega\tau - k^* \xi)\right], \tag{3.20}$$

$$F = \left[N_j \quad M_j \quad \Phi_E \quad \Psi\right]^T, \tag{3.21}$$

$$F_0 = \left[1 \quad 0 \quad 0 \quad 0\right]^T, \tag{3.22}$$

$$F_1 = \left[N_{j1} \quad M_{j1} \quad \Phi_{E1} \quad \Psi_1\right]^T. \tag{3.23}$$

In the auto-normalized Fourier form, $\Omega$ $\left(=\omega/\omega_{pl}\right)$ denotes the normalized fluctuation frequency and $k^*$ $\left(=k/2\pi\lambda_{Dl}^{-1}\right)$ designates the normalized wavenumber. In the Fourier transformed wave space $\left(\Omega, k^*\right)$, the spatial and temporal operators get transformed as $\partial/\partial\xi \to \left(ik^* - 1/\xi\right)$ and $\partial/\partial\tau \to (-i\,\Omega)$, respectively. The relevant fluid parameters appearing in equations (3.12)-(3.19) can respectively be written as

$$N_{e1} = -i\Omega^{-1}\left(ik^* + \xi^{-1}\right)M_{e1}\ , \tag{3.24}$$

$$M_{e1} = i\Omega\,\Phi_{E1}\left(ik^* - \xi^{-1}\right)\left[\left(k^{*2} + \xi^{-2}\right)\left(4^{-1}H'^{2}M_{Fe}^{2}k^{*2} - K'\gamma_e\right)\right]^{-1}, \tag{3.25}$$

$$N_{l1} = -i\Omega^{-1}\left(ik^* + \xi^{-1}\right)M_{l1}\ , \tag{3.26}$$

$$M_{l1} = -\sigma\mu\beta^{-1}k^{*-2}\left(k^{*2} + \xi^{-2}\right)\left(\Omega^2 + E\right)^{-1}M_{h1} - i\Omega\left(ik^* - \xi^{-1}\right)\left(\Omega^2 + E\right)^{-1}\Phi_{E1}\ \ , \tag{3.27}$$

$$N_{h1} = -i\Omega^{-1}\left(ik^* + \xi^{-1}\right)M_{h1}\ , \tag{3.28}$$

$$M_{h1} = \Phi_{E1}\left(-ik^* + \xi^{-1}\right)\left[-\sigma k^{*-2}\left(k^{*2} + \xi^{-2}\right)\left(\Omega^2 + E\right)^{-1} + \beta\right]\left[-i\Omega - i\Omega^{-1}H + \left(1 - i\Omega\tau_m^*\right)^{-1}\chi^* k^{*2}\right]^{-1}, \tag{3.29}$$

$$\Phi_{E1} = -k^{*-2}\left[(1+\mu)N_{e1} - N_{l1} - \mu N_{h1}\right], \tag{3.30}$$

$$\Psi_1 = -\sigma k^{*-2}\left(N_{l1} + \mu\beta^{-1}N_{h1}\right). \tag{3.31}$$

The substituted terms in equations (3.27) and (3.29) are given in an expanded form as

$$E = \left(k^{*2} + \xi^{-2}\right)\left\{\sigma k^{*-2} - A_l'\left(T^* + 2B_l^*\right)\right\}\ , \tag{3.32}$$

$$H = \left[2C_F^*\left(ik^* + \xi^{-1}\right) - A_h'\left(T^* + 2B_h^*\right)\left(k^{*2} + \xi^{-2}\right) + \sigma\mu\beta^{-1}k^{*-2}\left(k^{*2} + \xi^{-2}\right)\left\{-\sigma k^{*-2}\left(k^{*2} + \xi^{-2}\right)\left(\Omega^2 + E\right)^{-1} + 1\right\}\right]. \tag{3.33}$$

After a standard algebraic procedure of elimination and substitution in equations (3.24)-(3.31), we arrive at a septic dispersion relation given as

$$\Omega^7 + A_6\Omega^6 + A_5\Omega^5 + A_4\Omega^4 + A_3\Omega^3 + A_2\Omega^2 + A_1\Omega + A_0 = 0. \tag{3.34}$$

The different coefficients in equation (3.34) in an expanded form are cast as

$$A_6 = i\tau_m^{*-1}, \tag{3.35}$$

$$A_5 = \left(-k^{*2} + F\right)^{-1}\left(k^{*2} + \xi^{-2}\right)(1+\mu\beta) + \left(2E + Q - k^{*2}\chi^*\tau_m^{*-1}\right), \tag{3.36}$$

$$A_4 = i\tau_m^{*-1}\left[\left(-k^{*2} + F\right)^{-1}\left(k^{*2} + \xi^{-2}\right)(1+\mu\beta) + (2E+Q)\right], \tag{3.37}$$

$$\begin{aligned} A_3 = {} & \left(-k^{*2} + F\right)^{-1}\mu\left(k^{*2} + \xi^{-2}\right)\left(2E\beta - 2\sigma k^{*-2}\left(k^{*2} + \xi^{-2}\right) + E\mu^{-1}\right) + \left\{2E + \left(-k^{*2} + F\right)^{-1}\left(k^{*2} + \xi^{-2}\right)\right\}\left(Q - k^{*2}\chi^*\tau_m^{*-1}\right) \\ & + \left\{E^2 - \mu\beta^{-1}\left(\sigma k^{*-2}\left(k^{*2} + \xi^{-2}\right)\right)^2\right\}, \end{aligned} \tag{3.38}$$

$$\begin{aligned} A_2 = {} & i\tau_m^{*-1}\left[\left(-k^{*2} + F\right)^{-1}\mu\left(k^{*2} + \xi^{-2}\right)\left(2E\beta - 2\sigma k^{*-2}\left(k^{*2} + \xi^{-2}\right) + E\mu^{-1}\right) + \left\{2E + \left(-k^{*2} + F\right)^{-1}\left(k^{*2} + \xi^{-2}\right)\right\}Q\right] \\ & + i\tau_m^{*-1}\left[\left\{E^2 - \mu\beta^{-1}\left(\sigma k^{*-2}\left(k^{*2} + \xi^{-2}\right)\right)^2\right\}\right], \end{aligned} \tag{3.39}$$

$$\begin{aligned} A_1 = {} & \mu\beta^{-1}\left(k^{*2} + \xi^{-2}\right)\left\{\beta^2E^2\left(-k^{*2} + F\right)^{-1} - \sigma k^{*-2}\left(k^{*2} + \xi^{-2}\right)\left(2\beta E\left(-k^{*2} + F\right)^{-1} + \sigma k^{*-2}E\right)\right\} \\ & + \left\{E^2 + E\left(-k^{*2} + F\right)^{-1}\left(k^{*2} + \xi^{-2}\right)\right\}\left(Q - k^{*2}\chi^*\tau_m^{*-1}\right), \end{aligned} \tag{3.40}$$

$$\begin{aligned} A_0 = {} & i\tau_m^{*-1}\left[\mu\beta^{-1}\left(k^{*2} + \xi^{-2}\right)\left\{\beta^2E^2\left(-k^{*2} + F\right)^{-1} - \sigma k^{*-2}\left(k^{*2} + \xi^{-2}\right)\left(2\beta E\left(-k^{*2} + F\right)^{-1} + \sigma k^{*-2}E\right)\right\}\right] \\ & + i\tau_m^{*-1}\left[\left\{E^2 + E\left(-k^{*2} + F\right)^{-1}\left(k^{*2} + \xi^{-2}\right)\right\}Q\right]. \end{aligned} \tag{3.41}$$

We now apply the low-frequency approximation because we are interested to study the acoustic regime of the waves considered herein. In the ultra-low frequency limit ( $\Omega^a = 0 \forall\, a > 1$), equation (3.34) gets modified as

$$\Omega = iP\left[\left\{\left(E^2\left(-k^{*2}+F\right)+E\left(k^{*2}+\xi^{-2}\right)\right)\times k^{*2}\chi^{*}\right\}-\tau_m^{*}P\right]^{-1}. \quad (3.42)$$

The various substituted terms in equations (3.35)-(3.42) in generic notations are given as

$$F = (1+\mu)\left(4^{-1}H'^2M_{Fe}^2k^{*2}-K'\gamma_e\right)^{-1}, \quad (3.43)$$

$$Q = \left[2C_F^{*}\left(ik^{*}+\xi^{-1}\right)+\left(k^{*2}+\xi^{-2}\right)\left(\mu\beta^{-1}\sigma k^{*-2}-A_h'\left(T^{*}+2B_h^{*}\right)\right)\right], \quad (3.44)$$

$$P = \left[\mu\beta^{-1}\left(k^{*2}+\xi^{-2}\right)\left\{\beta^2E-\sigma k^{*-2}\left(k^{*2}+\xi^{-2}\right)\left(2\beta+\sigma k^{*-2}\left(-k^{*2}+F\right)\right)\right\}+\left\{E\left(-k^{*2}+F\right)+\left(k^{*2}+\xi^{-2}\right)\right\}Q\right]. \quad (3.45)$$

Thus, we see that the dispersion relation has major dependencies on different relevant effects considered herein, namely, the Bohm potential effect, Coriolis rotational force, radial distance, temperature, and so on.

### 3.4 RESULTS AND DISCUSSIONS

The semi-analytic study proposed herein puts forward a theoretic model to investigate the excitation and propagatory dynamics of the nucleus-acoustic waves in a rotating, self-gravitating, electrostatically confined degenerate quantum plasma system. The considered model is set up in the light of a spherically symmetric geometric construct. The concurrent influence of the Bohm potential, electrostatic confinement pressure, Coriolis rotation, self-gravity, and viscoelasticity is appropriately included. A linear normal mode analysis over the perturbed degenerate quantum plasma system yields a generalized dispersion relation (septic) of a unique pattern, characterizing the nucleus-acoustic waves excitable in the system. A numerical illustrative platform is provided to reveal the microphysical dynamics of the derived dispersion law, which is, in fact, validated in the ultra-low frequency approximation. The growth rates of the model system fluctuations with variation in the normalized wavenumber, with minor differences for both the non-relativistic and ultra-relativistic limits, are illustrated pictorially in figures 3.1-3.6.

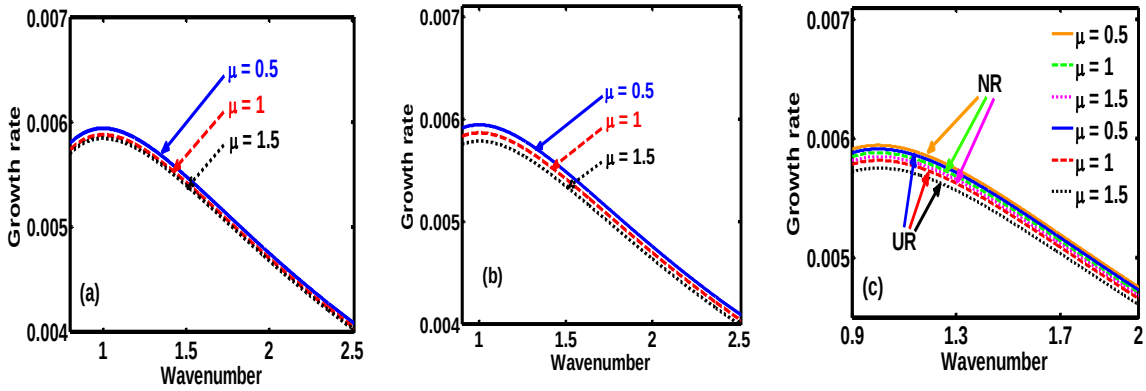


***Figure 3.1****: Profile of the normalized growth rate ($\Omega_i$) with variation in the normalized angular wavenumber ($k^*$) for different values of the charge density ratio of the heavy-to-light nuclear species ($\mu = Z_h n_{h0} / Z_l n_{l0}$). The different subplots link to the (a) non-relativistic (NR) limit, (b) ultra-relativistic (UR) limit, and (c) non-relativistic and ultra-relativistic limits respectively.*

In figure 3.1, we depict the profile structures of the growth rate with variation in the wavenumber for different values of the charge density ratio of the heavy-to-light nuclear species ($\mu = Z_h n_{h0} / Z_l\, n_{l0}$). The different subplots link to the (a) pure non-relativistic limit, (b) pure ultra-relativistic limit, (c) conjoint non-relativistic and ultra-relativistic limits, respectively. The different multiparametric input values used here are taken from the literature [1, 2, 7, 24, 26, 37] given as: $\sigma = 10^{-2}$, $\xi = 1$, $A_l' = 10$, $A_h' = 10^2$, $\tau_m^* = 10^{-2}$, $H' = 0.1$, $M_{Fe} = 1$, $\chi^* = 10^{-3}$, $C_F^* = 400$, $B_l^* = 4$, $B_h^* = 4$, $\beta = 1$. As clearly visible from the distinct coloured lines (figure 3.1), $\mu$ acts as a stabilizing agency for the fluctuations. It can be physically attributed to the dominancy of the inertial force imposed by the heavy nuclear species over the elasticity contributed conjointly by the light nuclear species and degenerate electronic species. Our model mimics the environment of a rapidly rotating contracting white dwarf star. If the contraction is large enough to increase the number density of heavy nuclei (number of nuclei present per unit volume), the value of $\mu$ gradually increases. The heavier nuclei are larger in size as compared to the lighter nuclei. It is because the nuclear size goes as, $R = f(A) = R_0 A^{1/3}$, where $R_0 = 1.2 \times 10^{-15}$ m and $A$ is the mass number of the nucleus. It is to be noted that the contraction in the dwarf plasma volume results in an increase in the number density of the lighter nuclei. It, however, results in more closeness of heavy

nuclei (bigger) than that of lighter nuclei (smaller). As a result, $\mu$ increases, thereby increasing the inertial action of the heavy nuclear species. Thus, $\mu$ introduces a stabilizing influence on the growth rate of the considered instability. For a better confirmatory visualization on a colour phase space ($k^*, \xi$), figure 3.2 shows the colourspectral profiles of the growth rate with variation in the radial distance and wavenumber for $\mu = 0.5$ in the (a) non-relativistic limit and (b) ultra-relativistic limit.

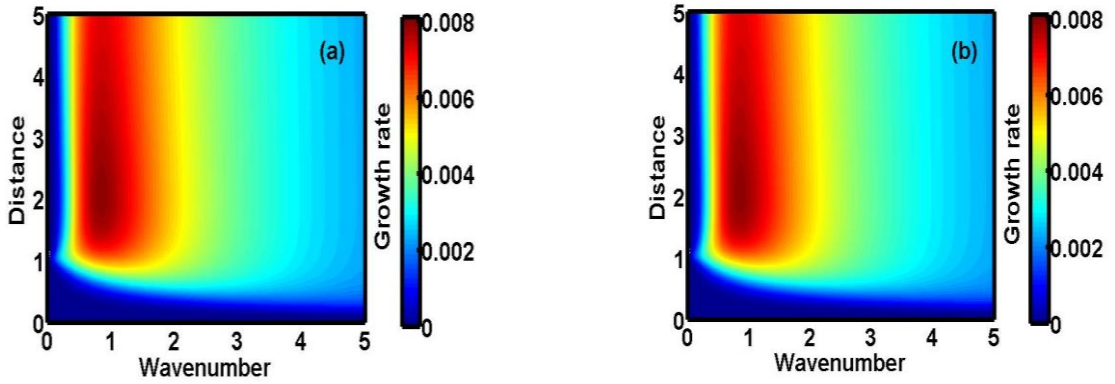


***Figure 3.2:*** *Colourspectral profile for the normalized growth rate for* $\mu = 0.5$ *in the (a) non-relativistic and (b) ultra-relativistic limits, respectively.*

As in figure 3.3, we show the same as figure 3.1, but for different values of the charge-to-mass coupling parameter ($\beta = Z_h m_l / Z_l m_h$). It is clearly seen that the growth rate increases gradually with $\beta$. Thus, it can be fairly concluded that $\beta$ introduces a destabilizing influence on the system. An increase in $Z_l / m_l$ ($\sim \beta^{-1}$) gradually increases the elastic effects provided conjointly by the degenerate electronic species and light nuclear species. Thus, decreasing $\beta$ should increase the nucleus-acoustic wave growth and vice-versa. But, a reverse is observed in both the non-relativistic (figure 3.3 (a)) and ultra-relativistic (figure 3.3 (b)) limits. It can be ascribed to the electrostatic confinement pressure effects, dominating more in weakly coupled plasmas [24, 37]. Higher the $Z_l / m_l$-value, higher is the electrostatic confinement pressure [24, 37] (due to higher $B_l$); and vice-versa. Thus, an enhanced electrostatic confinement pressure suppresses the instability growth (higher-$Z_l / m_l$, lower-$\beta$); and

vice-versa. Similarly, figure 3.4 depicts the colourspectral profiles of the growth rate as figure 3.2, but for $\beta = 0.5$.

In a similar manner, figure 3.5 shows the same as figure 3.1, but for different values of the Coriolis rotation force. The distinct coloured lines clearly indicate that an increase in the Coriolis force results in an enhanced growth rate, in both the non-relativistic (figure 3.5(a)), and ultra-relativistic (figure 3.5(b)) limits. The Coriolis rotation destabilizes the system subject to the conjoint action of the concurrent effects of the considered factors simultaneously. The physical insight behind this is grounded on the fact that, greater the mass of the system, greater is the angular momentum, thereby leading to a higher degree of the Coriolis rotation. It is well established in the diversified astrocosmical scenarios that heavier objects gravitationally collapse faster, and vice-versa. It hereby enables us to infer that the Coriolis rotational force plays an active role in the destabilization process of the system against the non-local long-range gravity. Lastly, figure 3.6 depicts almost the same features as figure 3.4, but for $C_F^* = 400$. It is noted that there exists some minor quantitative disparities ascribable to the parametric domains under analysis.

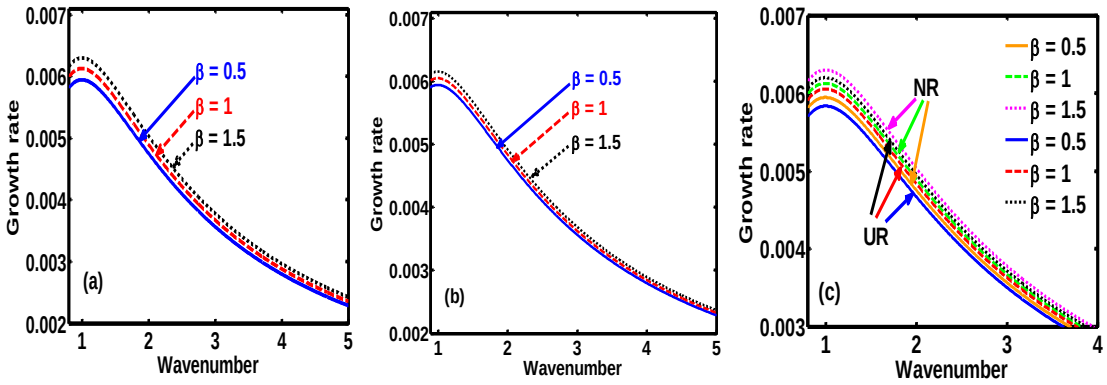


***Figure 3.3****: Same as figure 3.1, but for different values of charge-to-mass coupling parameter ( $\beta = Z_h m_l / Z_l m_h$ ) in the (a) non-relativistic limit, (b) ultra-relativistic limit, (c) non-relativistic and ultra-relativistic limits, respectively.*

It may be noteworthy that, figures 3.2, 3.4, 3.6 are the colourspectral profiles obtained by changing the Matlab camera's line of sight (i.e., orientation or projection) of the three-dimensional surface plots (with the wavenumber, distance, growth rate taken in three mutually independent perpendicular axes with a common origin). The

actual three-dimensional surfaces are developed methodologically by executing the full numerical simulation of the generalized linear dispersion relation (septic in degree), given by equation (3.34), which is reduced in the low-frequency regime as equation (3.42), in the platform of the Matlab programming. More technically, these three-dimensional figures are developed with the azimuthal and the elevation angles set equal to 0 and 90, respectively. Against this backdrop, it is already evident that figures 3.1, 3.3, 3.5 are simply the two-dimensional spectral profiles obtained by the same dispersion analysis (with the wavenumber and growth rate taken in two independent perpendicular axes with a common origin).

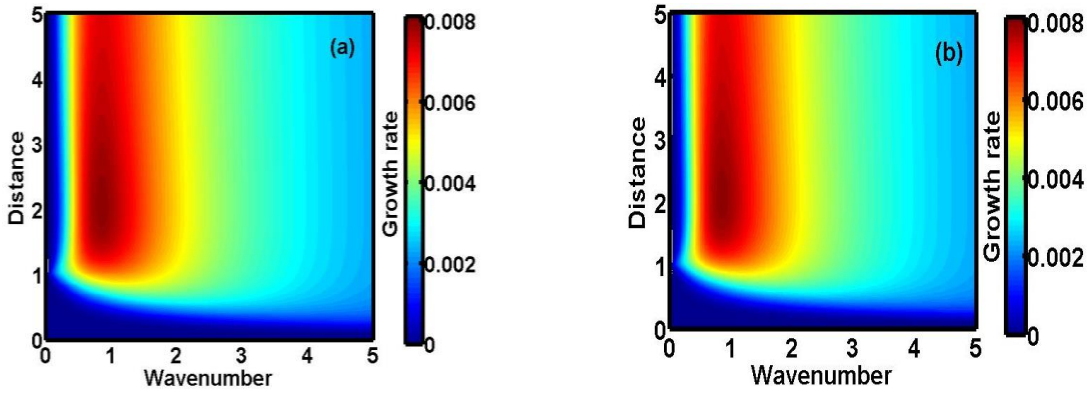


***Figure 3.4****: Same as figure 3.2, but for* $\beta = 0.5$ *in the (a) non-relativistic limit and (b) ultra-relativistic limit, respectively.*

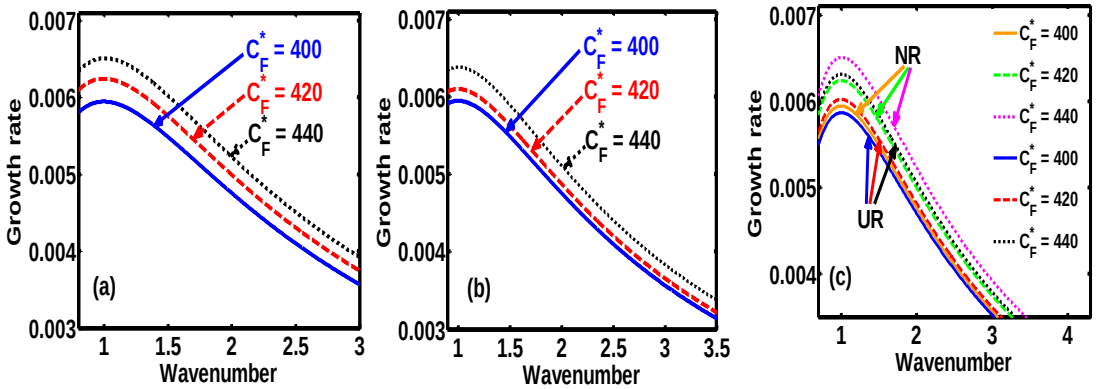


***Figure 3.5****: Same as figure 3.1, but for different values of the Coriolis force* ***(*** $C_F^*$ ***)*** *in the (a) non-relativistic limit, (b) ultra-relativistic limit, (c) non-relativistic and ultra-relativistic limits, respectively.*

The obtained results, mainly on the Coriolis rotational role as a destabilizing agency, are fairly correlative and consistent with the previous astronomical findings on the gyratory compact astroobjects, as widely evident in the literature [26]. In fact, it has been practically found in the case of a white dwarf stars, like SS Cygni, CM Del, and so forth that its rotational speed fairly increases during the unstable outburst phase, which reliably hints at the concretized accuracy of our proposed model analysis depicting rotation-induced destabilizing effects in such astrocompact circumstances.

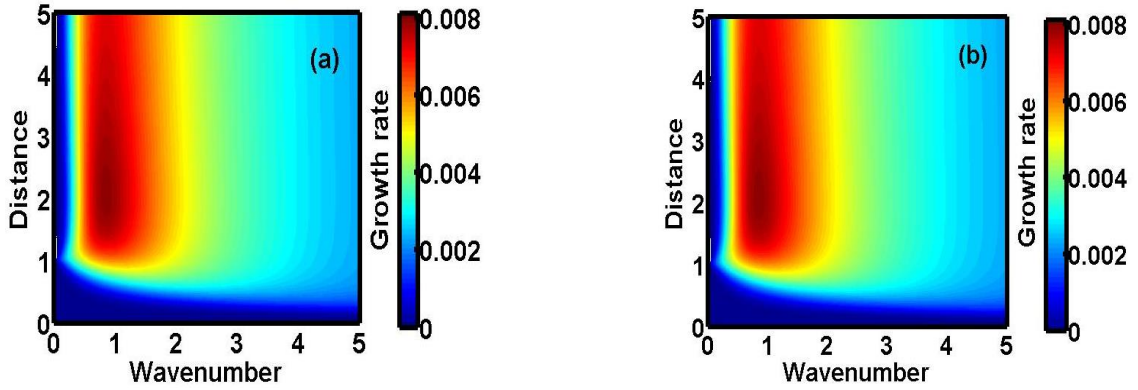


***Figure 3.6****: Same as figure 3.2, but for* $C_F^* = 400$ *in the (a) non-relativistic limit and (b) ultra-relativistic limit, respectively.*

The above analysis is restricted to the excited wave instability features just in the core and mantle of a rapidly rotating collapsing white dwarf stellar configuration, where the dominance of the three considered species (degenerate electronic species, light nuclear species, heavy nuclear species) indeed prevails [11-13]. The crust and atmosphere of the white dwarfs consist of alkali metals, mainly lithium (Li) and potassium (K) [40], where our analysis would not be so appropriate to apply. It may be pertinent to add furthermore that the composition of the crust and atmosphere of degenerate white dwarfs can similarly be mapped to that of rocky planets, such as the Earth, Mars, and so forth [40]. Thus, the main limitation of our generalized hydrodynamic model-based study is the fact that the model analysis cannot be applied to the classical crust and atmosphere of a white dwarf star due to the postulated compositional disparity. Besides, the adopted idealized consideration of a spherically symmetric geometry with the polar and azimuthal wave-kinetic aspects completely ignored gives a clear indication for the future scope of a judicious model refinement in

this direction. Extensive applicability of the analysis, despite the above facts and faults, may be relevant in the viscous evolution of white dwarf merger remnants [34].

### 3.5 CONCLUSIONS

The theoretic analysis presented in this Chapter puts forward a semi-analytic model formulation to study the excitation and propagation dynamics of the nucleus-acoustic waves in a compact astrophysical fluid system. The model is founded in a generalized hydrodynamic fabric practically resembling white dwarf interior environs. It considers a three-component plasma system composed of heavy nuclear species, light nuclear species and tiny quantum degenerate electronic species. It is under the simultaneous action of the Bohm potential, Coriolis rotational force, electrostatic confinement pressure, self-gravity, and viscoelasticity. A standard normal spherical mode analysis over the perturbed degenerate quantum plasma system yields a generalized linear dispersion relation (septic). It highlights the explicit dependency of various atypical parametric constants on the diversified equilibrium plasma properties. A numerical illustrative platform is provided to explore the multiparametric influential dependencies of the degenerate quantum plasma fluctuation dynamics in detail. It presents different relevant two-dimensional growth-damping profiles (figures 3.1, 3.3, 3.5) and the corresponding colourspectral profiles (figures 3.2, 3.4, 3.6) with some minor quantitative differences in the non-relativistic and ultra-relativistic regimes of the electronic dynamics with wide astrocosmic relevance.

The main conclusions drawn from this study include the fact that, in both the non-relativistic and ultra-relativistic limits, the charge density ratio of the heavy-to-light nuclear species ($\mu$) introduces a stabilizing influence on the system (figure 3.1). The charge-to-mass coupling parameter ($\beta$) destabilizes the system (figure 3.3). It can be further inferred from the proposed model analysis that the Coriolis rotation destabilizes the system (figure 3.5). The physical insights responsible behind are concisely illuminated in the relevant perspectives. It is substantiated fairly by the observed astronomical data [25, 26, 30], which, reinforcingly, hint at the same Coriolis rotational effects, as investigated here.

White dwarfs are extremely compact astrophysical objects where the gravitational attraction is balanced by the non-thermal degenerate electronic pressure.

Thus, degenerate electronic pressure plays a significant role throughout the life of a white dwarf star. The effect of viscoelastic dissipation is mainly visible for strongly coupled heavy nuclear species in the parameter space defined by $0 < \tau_m < \infty$ [38]. Also, for a rapidly rotating contracting white dwarf star approaching collapse, material in the envelope is shed when $v_c^2/2 = \left(GM^* M_\Theta\right)/R_c$; where, $M^*$ is the normalized mass of the star on the $M_\Theta$-scale, $R_c$ is the equatorial radius of the white dwarf star, and $v_c$ is the equatorial velocity [33]. At this stage of collapse, the material in rapidly rotating white dwarf stars is highly viscoelastic [33]. A significant fraction of mass of white dwarf merger remnants is initially supported by rotation. Post merger viscous phase causes detonation of the helium (He) envelope in white dwarf mergers [34], thereby acting as potential triggering agents of Type-Ia supernovae. Thus, the obtained results may prove to be beneficial in understanding the diversified wave features in compact astroobjects, interiors, and correlated surroundings. It especially refers to white dwarfs, where the effects of viscoelastic dissipation, degenerate electron pressure, and strongly correlated inertial heavy nuclear species play a crucial role.

It has been reported that there exist a rich plethora of more than hundred oscillation (pulsation) modes, both in pre-white dwarf stars, such as PG1159-035 [13], and in variable white dwarf stars, such as GD-358 [13]. It has left behind an interesting scope for the future discovery of different collective waves, instabilities, and their saturation structures in such plasma media, with the proposed nucleus-acoustic waves and propagatory dynamics as their special cases in extreme conditions as proposed herein. Lastly, it is reiterated that our results may have concrete and promising applications in understanding the evolution, excitation, and propagation dynamics of the nucleus-acoustic and similar normal acoustic modes widely supported in compact correlated astroobjects and their correlated interiors.

**REFERENCES**


[1] Karmakar, P. K. and Das, P. Nucleus-acoustic waves: Excitation, propagation, and stability. *Phys. Plasmas*, 25, 082902, 2018.

[2] Das, P. and Karmakar, P. K. Nonlinear nucleus-acoustic waves in strongly coupled degenerate quantum plasmas. *Europhysics Letters*, 126, 10001p1-10001p7, 2019.

[3] Haas, F. *Quantum Plasmas- A hydrodynamic approach*, Springer, New York, 2011.

[4] Khan, S. A. and Bonitz, M. Quantum hydrodynamics. in *Complex Plasmas: Scientific Challenges and Technological Opportunities*, pages 103-152, Springer, 2014.

[5] Chabrier, G., Saumon, D., and Potekhin, A. Y. Dense plasmas in astrophysics: from giant planets to neutron stars. *Journal of Physics A: Mathematical and General*, 39, 4411-4419, 2006.

[6] Manfredi, G. How to model quantum plasmas. *Field Institute Communications*, 46:263-287, 2005.

[7] Zaman, D. M. S., Amina, M., Dip, P. R. and Mamun, A. A. Planar and non-planar nucleus-acoustic shock structures in self-gravitating degenerate quantum plasma systems. *European Physical Journal Plus*, 132, 457, 2017.

[8] Mannan, A. Theory for nucleus-acoustic waves in warm degenerate quantum plasmas. *Reviews of Modern Plasma Physics*, 6:3, 2022.

[9] Chandrasekhar, S. The density of white dwarf stars. *Philosophical Magazine*, 11 (70): 592-596, 1931.

[10] Chandrasekhar, S. The maximum mass of ideal white dwarfs. *The Astrophysical Journal*, 74:81-82, 1931.

[11] Koester, D. and Chanmugam, G. Physics of white dwarf stars. *Reports on Progress in Physics*, 53(7): 837-915, 1990.

[12] Vennes, S. and Kawka, A. The core composition of a white dwarf in a close double-degenerate system. *The Astrophysical Journal Letters*, 745(1)**:**L12, 2012.

[13] Koester, D. White dwarfs: Recent developments. *The Astronomy and Astrophysics Review*, 11:33-66, 2002.

[14] Mamun, A. A., Amina, M., and Schlickeiser, R. Nucleus-acoustic shock structures in a strongly coupled self-gravitating degenerate quantum plasma. *Physics of Plasmas*, 23:094503, 2016.

[15] Mamun, A. A., Amina, M., and Schlickeiser, R. Heavy nucleus-acoustic spherical solitons in self-gravitating super-dense plasmas. *Physics of Plasmas*, 24:042307, 2017.

[16] Mamun, A. A. Degenerate pressure driven modified nucleus-acoustic waves in degenerate plasmas. *Physics of Plasmas*, 25: 024502, 2018.

[17] Sultana, S., Islam, S., Mamun, A. A., and Schlickeiser, R. Modulated heavy nucleus-acoustic waves and associated rogue waves in a degenerate relativistic quantum plasma system. *Physics of Plasmas*, 25: 012113, 2018.

[18] Chowdhury, N. A., Hasan, M. M., Mannan, A., and Mamun, A. A. Nucleus-acoustic envelope solitons and their modulational instability in a degenerate quantum plasma system. *Vacuum*, 147:31-37, 2018.

[19] Saaduzzaman, D. M., Amina, M., and Mamun, A. A. Nucleus-acoustic Solitons in Self-gravitating Magnetized Quantum Plasmas. *Journal of the Physical Society of Japan*, 87, 034502, 2018.

[20] Jannat, S. and Mamun, A. A. Nucleus-acoustic solitary waves in white dwarfs. Chinese Journal of Physics, 56(6): 3043-3052, 2018.

[21] Jannat, S. and Mamun, A. A. Nucleus-acoustic shock waves in white dwarfs. *Pramana – Journal of Physics*, 90:51, 2018.

[22] Zaman, D. M. S., Amina, M., Dip, P. R., and Mamun, A. A. Nucleus-acoustic solitary waves in self-gravitating degenerate quantum plasmas. *Chinese Physics B*, 27(4):040402, 2018.

[23] Mannan, A., Sultana, S., and Mamun, A. A. Arbitrary Amplitude Heavy Nucleus-Acoustic Solitary Waves in Thermally Degenerate Plasmas. *IEEE Transactions on Plasma Science*, 48(12): 4093-4102, 2020.

[24] Shukla, M. K., Avinash, K., Mukherjee, R., and Ganesh, R. Isothermal equation of state of three dimensional Yukawa gas. *Physics of Plasmas*, 24:11304, 2017.

[25] Kawaler, S. White Dwarf Rotation: Observations and Theory. In *Stellar Rotation, Proceedings of IAU symposium No. 215*, Cancun, Mexico, 2003.

[26] Livio, M. and Pringle, J. E. The rotation rates of white dwarfs and pulsars. *The Astrophysical Journal*, 505(1):339-343, 1998.

[27] Lang, K. R. *Essential Astrophysics*. Springer, New York, 2013.

[28] Dutta, P. and Karmakar, P. K. Dynamics of gravoviscothermal instability in complex astrofluids amid cosmic radiative moderation effects. *Astrophysics and Space Science*, 364:217, 2019.

[29] Kalita, D. and Karmakar, P. K. Analyzing the instability dynamics of spherical complex astroclouds in a magnetized meanfluidic fabric. *Physics of Plasmas*, 27:022902, 2020.

[30] Mauche, C. W. The quasi-coherent oscillations of SS Cygni. In *Accretion Phenomenon and Related Outflows, IAU Colloquium 163, ASP conference series,* volume 121, pages 251-255, Port Douglas, Australia, 1997.

[31] Chen, F. F. *Introduction to plasma physics and controlled fusion*. Plenum press, New York, 2nd edition, 1984.

[32] Mushtaq, A. Ion acoustic solitary waves in magneto-rotating plasmas. *Journal of Physics A: Mathematical and Theoretical,* 43:315501, 2010.

[33] Monaghan, J. J. The structure of rapidly rotating white dwarfs. *Monthly Notices of the Royal Astronomical Society.* 132(2):305-316, 1966.

[34] Schwab, J., Shen, K. J., Quataert, E., Dan, M., and Rosswog, S. The viscous evolution of white dwarf merger remnants. *Monthly Notices of the Royal Astronomical Society***.** 427(1): 190-203, 2012.

[35] Camenzind M. *Compact Objects in Astrophysics: White Dwarfs, Neutron Stars and Black Holes,* Springer, New York, 2007.

[36] Karmakar, P. K. and Das, P. Instability analysis of cosmic viscoelastic gyro-gravitating clouds in the presence of dark matter. *Astrophysics and Space Science,* 362:142, 2017.

[37] Shukla, M. K. and Avinash, K. Equilibrium configuration of self-gravitating charged dust clouds: Particle approach. *Physics of Plasmas*, 26:013701, 2019.

[38] Kaw, P. K. and Sen, A. Low frequency modes in strongly coupled dusty plasmas. *Physics of Plasmas*, 5:3552, 1998.

[39] Daligault, J. and Sjostrom, T. *Dense plasma theory: Microphysical properties of dense, strongly coupled, and quantum plasmas.* Retrieved on 18 Dec. 2020 from https://www.lanl.gov/projects/dense-plasma-theory/background/physical-regimes.php

[40] Hollands, M. A., Tremblay, P. E., Gänsicke, B. T., Koester, D., and Gentile-Fusillo, N. P. Alkali metals in white dwarf atmospheres as tracers of ancient planetary crusts. *Nature Astronomy*, **5**:451-459, 2021.